DFT and Kinetic Monte Carlo Study of TMS-Substituted Ruthenium Vinyl Carbenes: Key Intermediates for Stereoselective Cyclizations

ARTICLE *in* ACS CATALYSIS · SEPTEMBER 2015

Impact Factor: 9.31 · DOI: 10.1021/acscatal.5b01333

4 AUTHORS, INCLUDING:

Fermín Cambeiro

University of Santiago de Compostela

6 PUBLICATIONS **35** CITATIONS

SEE PROFILE

Emilio Martinez-Nuñez

University of Santiago de Compostela

85 PUBLICATIONS **1,019** CITATIONS

SEE PROFILE

Jesús A. Varela

University of Santiago de Compostela

51 PUBLICATIONS **1,232** CITATIONS

SEE PROFILE

ACS Catalysis

Research Article

pubs.acs.org/acscatalysis

DFT and Kinetic Monte Carlo Study of TMS-Substituted Ruthenium Vinyl Carbenes: Key Intermediates for Stereoselective Cyclizations

Fermín Cambeiro,[†] Emilio Martínez-Núñez,[‡] Jesús A. Varela,*[,†] and Carlos Saá*[,†]

[†]Departamento de Química Orgánica y Centro Singular de Investigación en Química Biológica y Materiales Moleculares (CIQUS) and [‡]Departamento de Química Física y Centro Singular de Investigación en Química Biológica y Materiales Moleculares (CIQUS), Universidad de Santiago de Compostela, 15782 Santiago de Compostela, Spain

Supporting Information

ABSTRACT: Mechanistic pathways for the cyclization of 1,5-alkynylacetal with N_2CHTMS in the presence of Cp- and Cp*RuCl(cod) to afford (*Z*)- and (*E*)-(trimethylsilyl)vinyl spiroacetals have been calculated. Calculations show the presence of three conformers in equilibrium for the initially formed ruthenium carbenes. Differences in the stabilities and reactivities of the conformers, depending on the use of a Cp or Cp* ruthenium catalyst, are responsible for the favorable active reaction pathways in each case, even though the geometry of the resulting product is the same regardless of the catalyst used. Kinetic Monte Carlo (KMC) simulations with rate coefficients, including tunneling probabilities for the hydride transfer step, were used to model the evolution of reactants, intermediates, and products for all calculated pathways. It was shown that one path is almost exclusively active for each catalyst. Finally, the energetic span model of Kozuch and Shaik was used to calculate the energetic span (δE), the TOF-determining transition state (TDTS), the TOF-determining intermediate (TDI), and the TOF value for each of the feasible mechanistic pathways.

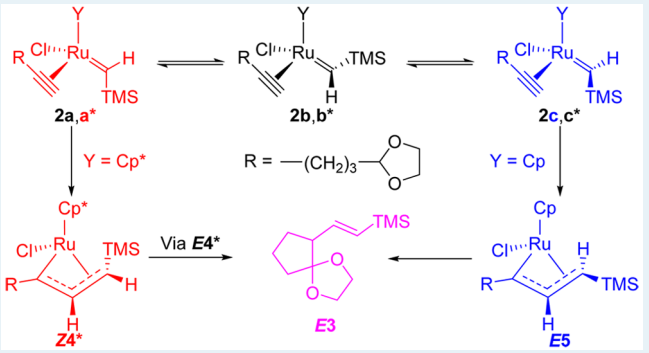

KEYWORDS: *density functional calculations, energetic span model, kinetic Monte Carlo simulations, ruthenium vinyl carbenes, TOF*

1. INTRODUCTION

Metal carbene complexes have proven their value in organic synthesis due to the number of catalytic organometallic transformations in which they are involved. For example, such complexes have been investigated in a wide variety of alkene metathesis transformations such as cross metathesis (CM), ring-closing metathesis (RCM), acyclic diene metathesis (ADMET), and ring-opening metathesis polymerization (ROMP),[1] as well as in reactions with alkynes such as alkyne polymerization,[2] enyne metathesis,[3] cyclopropenation,[4] etc. Recently, the formation of substituted ruthenium vinyl carbene intermediates under mild conditions by treatment of functionalized alkynes with diazoalkanes in the presence of the precatalyst Cp*RuCl(cod) has been described.[5] Interestingly, the nature of the reaction products is strongly dependent on the alkyne functionality, whereas the stereoselectivity is more affected by subtle structural features in both the diazoalkanes and substrates (Scheme 1): (a) simple alkynes[6] and (b) propargylic carboxylates[7] furnished mixtures of 1,3-dienes by double carbene addition to the triple bond, coupling of the carbene with the alkyne terminal carbon, and a 1,2-shift of the carboxylate, respectively, (c) enynes with terminal triple bonds led to mixtures of diastereomers of alkenyl bicyclo[*x*.1.0]-alkanes,[8] (d) 1,6-enynes disubstituted at the propargylic positions afforded alkenyl alkylidene cyclopentanes;[8] (e) 1,6-allenynes were converted to *E*,*Z*-mixtures of alkenyl alkylidene bicyclo[3.1.0]hexanes,[9] (f) alkynyl acetals, ethers and amines afforded complex *E* isomers of spiro and fused bicyclic structures by an intramolecular neutral redox process that involves hydride transfer to the carbene,[10] and (g) nucleophilic attack of carbonyl nucleophiles to the carbene center led to *Z* isomers of 2-vinyldihydropyrans.[11]

The mechanistic hypotheses are all based on the initial generation of the 16e ruthenium carbene intermediate **B** by displacement of the cod ligand of precatalyst **A** with the diazoalkane and concomitant release of N_2. Subsequent coordination of the alkyne followed by a facile [2 + 2] cycloaddition would give rise to the ruthenacyclobutene **C**, which would undergo a cycloreversion to the ruthenium vinyl carbene **D**, in which the alkene geometry is not easily predictable (Scheme 2).[1]

The stereochemistry of this double bond is determined, according to the proposed mechanism, during the electrocyclic opening of the ruthenacyclobutene **C**, in which the Cp* and Y groups should be anti to avoid unfavorable steric interactions. Thus, if Y = $SiMe_3$ a *Z* configuration is favored because strong

Received: June 25, 2015
Revised: September 8, 2015

DOI: 10.1021/acscatal.5b01333
ACS Catal. 2015, 5, 6255−6262

Scheme 1. *E,Z* Geometries for Alkenes Obtained from Catalytic Cp*RuCl(cod) and Diazo Compounds with (a) Alkynes, (b) Propargylic Carboxylates, (c) Enynes, (d) 1,6-Enynes, (e) 1,6-Allenynes, (f) Alkynyl Acetals, Ethers, and Amines, and (g) Alkynals and Alkynones

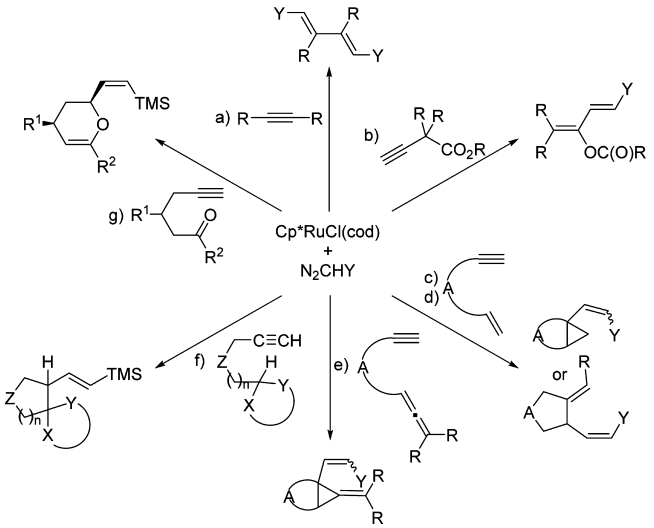

Scheme 2. Mechanistic Hypothesis for the Formation of Ruthenium Vinyl Carbenes

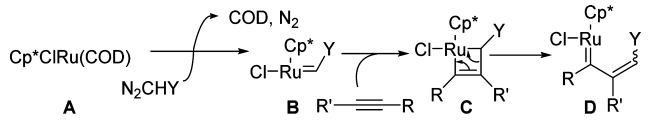

interactions are established between $SiMe_3$ and Cl groups. On the other hand, if Y ≠ $SiMe_3$, then steric interactions are the major factors and this leads to the *E* configuration (Scheme 3).[6,7]

Scheme 3. (*Z*)- and (*E*)-Vinyl Carbenes by Ring Opening of Ruthenacyclobutenes

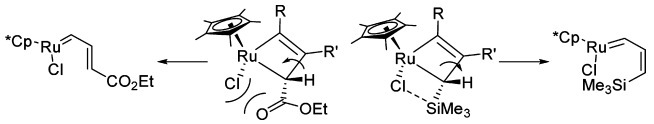

Nevertheless, treatment of alkynyl acetals, ethers, and amines with N_2CHY (Y = TMS) in the presence of catalytic amounts of Cp*RuCl(cod) gave, in most cases, the corresponding cyclic compounds with an *E* configuration on the vinylsilane group. A hydride transfer from a C_{sp^3}–H to an initially formed ruthenium (trimethylsilyl)vinyl carbene with *E* geometry might be involved (Scheme 4).[10]

In an effort to explain these apparent geometrical discrepancies, we present here a detailed theoretical mechanistic study using DFT calculations for the reaction of alkynyl acetal **1** with (trimethylsilyl)diazomethane in the presence of Cp- or Cp*RuCl(cod) to afford the corresponding spiroacetals ***Z*3** and ***E*3** (Scheme 5). The calculated theoretical rate for each step in the catalytic cycle would allow the determination of the most favorable pathway using kinetic Monte Carlo (KMC) simulations, as well as the theoretical TOF of the catalytic cycle. Special attention was paid to the geometrical isomer formed.

Scheme 4. Spirocyclic and Bicyclic Compounds from Ruthenium Vinyl Carbenes

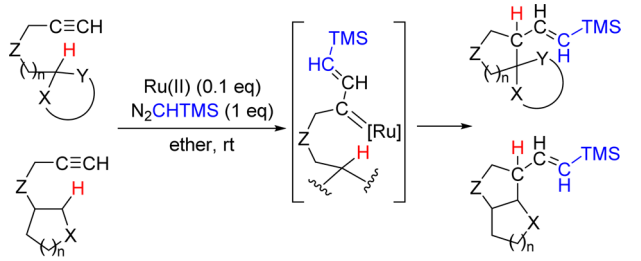

Scheme 5. Spiroacetals from Ruthenium-Catalyzed Cyclization of Alkynylacetals with (Trimethylsilyl)diazomethane

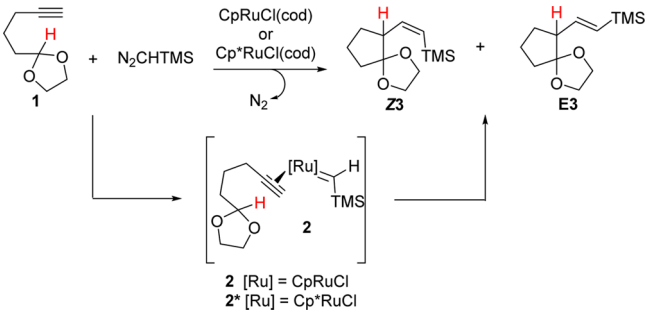

2. COMPUTATIONAL DETAILS

All electronic structure calculations were performed using the Gaussian 09 software package[12] at the CESGA facilities. The geometries of all minima and transition states involved were optimized at the B3LYP[13] level with the double-ζ LANL2DZ[14] basis set and the LANLD2Z pseudopotential[15] to describe the electrons of the ruthenium atom. The 6-31G(d) basis set was employed for all other atoms.[16] Frequency calculations were performed at the same level to evaluate the zero-point vibrational energy and thermal corrections at 298 K and to confirm the nature of the stationary points, yielding one imaginary frequency for the transition states and none for the minima. Each transition state was further confirmed by following the steepest descent to both sides and identifying the minima present in the reaction energy profile. Single-point energies were calculated using B3LYP with the addition of Grimme's D3 dispersion corrections[17] (B3LYP-D3) within the self-consistent reaction field (SCRF) using the SMD model (diethyl ether)[18] with the same basis set and pseudopotential for the ruthenium atom and 6-311++G(d,p)[19] for all other atoms. The resulting energies were used to correct the gas-phase energies obtained from B3LYP calculations. The reaction profiles were built up in terms of ΔG_{sol}.

Kinetic Monte Carlo (KMC) simulations[20] were employed to model the time evolution of reactants, intermediates, and products. KMC is a very useful Monte Carlo simulation for modeling the transient behavior of various molecular species that participate in many highly coupled steps. The thermal rate constants $k(T)$ for each individual step, which give the probability of taking a particular path in the KMC run, are calculated from the Eyring transition state theory (TST) expression:[21]

$$k(T) = \kappa \frac{k_B T}{h} e^{-\Delta G^{\ddagger}/RT}$$

DOI: 10.1021/acscatal.5b01333
ACS Catal. 2015, 5, 6255–6262

where k_B is the Boltzmann constant and κ is the transmission coefficient. In this study the temperature T was set to 298 K and the transmission coefficient was 1 for all steps, except for the hydride-transfer reactions. In these cases, the Eckart potential[22] was employed to compute the tunneling probabilities, which can then be integrated to obtain the transmission coefficient.[23]

3. RESULTS AND DISCUSSION

First, a conformational study of the ruthenium−carbene bond[24] of the initially formed carbene **2** ([Ru] = CpRuCl) was carried out (Scheme 5). Three minimum conformations were found: complex **2a**, which has the TMS group opposite to the Cp ring, complex **2b**, which has the TMS group away from the ruthenium alkyne ligand (ΔG° = 1.1 kcal mol^{-1} less stable than **2a**), and complex **2c**, which has the TMS group close to the ruthenium alkyne ligand (ΔG° = 0.3 kcal mol^{-1} more stable than **2a**). The values for the Gibbs free energy of activation $\Delta G^\ddagger$ found for the rotation of the carbene−ruthenium bond (4.9, 2.0, and 4.9 kcal mol^{-1} for the transformation **2a** → **2b** → **2c** → **2a**) indicate that all carbene conformers are present in the initial equilibrium (Figure 1).

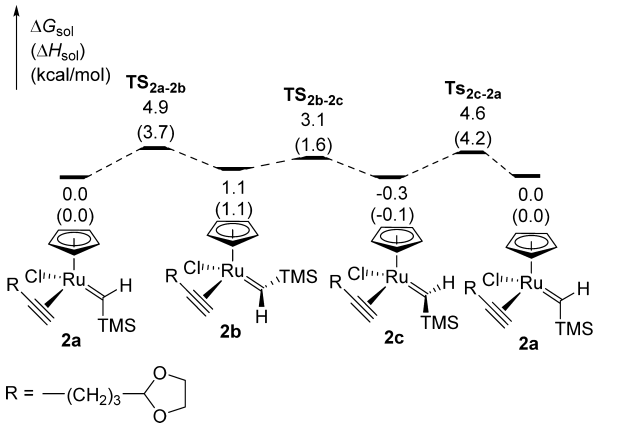

Figure 1. Free energy profile for the conformational analysis of ruthenium carbene **2**. Energies are relative to **2a** and are mass balanced.

The [2 + 2] cycloadditions between the alkyne and the Ru carbene from conformers **2a,c** were subsequently analyzed.[25] In both cases, a η^3-vinyl carbene complex was obtained instead of a ruthenacyclobutene; thus, from **2a** the η^3-vinyl carbene ***Z*4** was obtained with ΔG° = −29.3 kcal mol^{-1} and $\Delta G^\ddagger$ = 6.6 kcal mol^{-1} and from **2c** the η^3-vinyl carbene ***E*5** was produced with ΔG° = −34.0 kcal mol^{-1} and $\Delta G^\ddagger$ = 5.1 kcal mol^{-1} (Figure 2).[26] According to the Curtin−Hammett principle,[27] when two products are irreversibly formed at different reaction rates from two conformers in equilibrium, the observed product distribution will not reflect the equilibrium distribution of the conformers. Thus, the mechanistic study was continued from the two isomers ***Z*4** and ***E*5**.

Once ***Z*4** and ***E*5** had been formed, it was possible to find a path for their isomerization to ***E*4** and ***Z*5**, respectively (Figure 3). In the case of ***Z*4**, this isomerization occurs in two steps: transformation of ***Z*4** into the intermediate ruthenacyclobutene **I**, in which the TMS group and the Cp ring are trans (ΔG° = 11.0 kcal mol^{-1} and $\Delta G^\ddagger$ = 17.5 kcal mol^{-1}), and transformation of **I** to ***E*4** (ΔG° = −13.9 kcal mol^{-1} and $\Delta G^\ddagger$ = 3.9 kcal mol^{-1}). On the other hand, the much more unfavorable

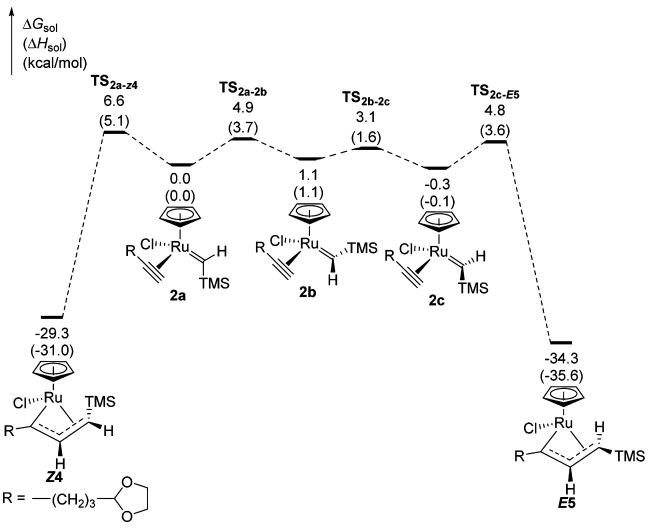

Figure 2. Free energy profile for the formation of ***Z*4** and ***E*5** from **2a,c**, respectively. Energies are relative to **2a** and are mass balanced.

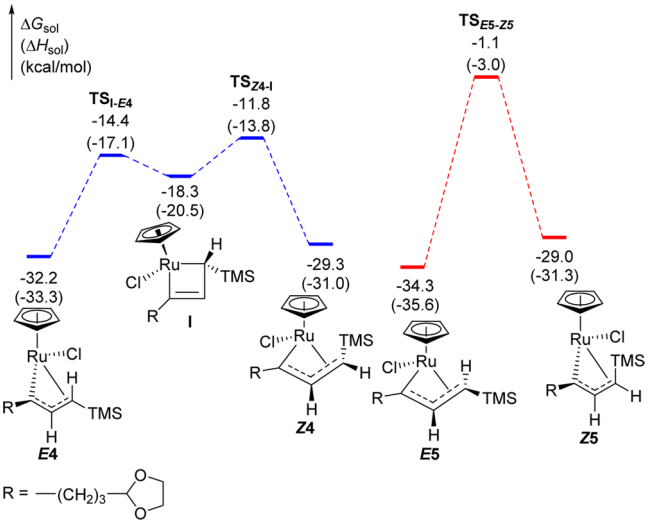

Figure 3. Free energy profiles for the isomerization of ***Z*4** and ***E*5** into ***E*4** and ***Z*5** through Cp ruthenacyclobutenes **I** and $\mathbf{TS}_{E5\text{-}Z5}$, respectively. Energies are relative to **2a** and are mass balanced.

transformation of ***E*5** to ***Z*5**, both thermodynamically and kinetically, occurs in only one step with ΔG° = 5.3 kcal mol^{-1} and $\Delta G^\ddagger$ = 33.2 kcal mol^{-1}. In this last transformation, the ruthenacyclobutene that is analogous to **I**, but with the TMS group cis to the Cp ring, was found to be the transition state $\mathbf{TS}_{E5\text{-}Z5}$, probably due to the instability caused by the cis disposition of the TMS and the Cp ring.

In summary, the two structures ***Z*4** and ***E*4** can be envisaged as resulting from the two possible ring-opening conrotatory electrocyclizations of the ruthenacyclobutene **I** (TMS and Cp trans), whereas ***E*5** and ***Z*5** would result from the same reaction type on the transition state $\mathbf{TS}_{Z5\text{-}E5}$ (structurally analogous to intermediate **I** but with TMS and Cp cis to one another). Therefore, the spiroacetal ***Z*3** will arise from the hydride transfer to the ruthenium carbene in species ***Z*4** and ***Z*5** while spiroacetal ***E*3** will arise from ***E*4** and ***E*5**.

In order to facilitate the hydride transfer to the ruthenium carbene, it is necessary to place the hydrogen in an appropriate position, which requires a prior conformational change of the

DOI: 10.1021/acscatal.5b01333
ACS Catal. 2015, 5, 6255−6262

alkynyl acetal ligand. The energetically most favorable conformations would be those that allow a six-membered transition state in a chair conformation. Considering that there are two chairlike conformations and that the hydride can attack the carbene at either the *Si* or *Re* face, there are a total of 16 different geometries suitable for the hydride transfer: i.e., four for each isomer. For example, in the case of ***Z*4** there are two possible conformers, ***Z*4a**$_{Si}$ and ***Z*4b**$_{Si}$, for the attack of the hydride on the *Si* face of the Ru carbene and two other conformers, ***Z*4a**$_{Re}$ and ***Z*4b**$_{Re}$, in the case of attack on the *Re* face (Figure 4). For the other isomers, ***E*4**, ***E*5**, and ***Z*5**, an analogous nomenclature will be used.

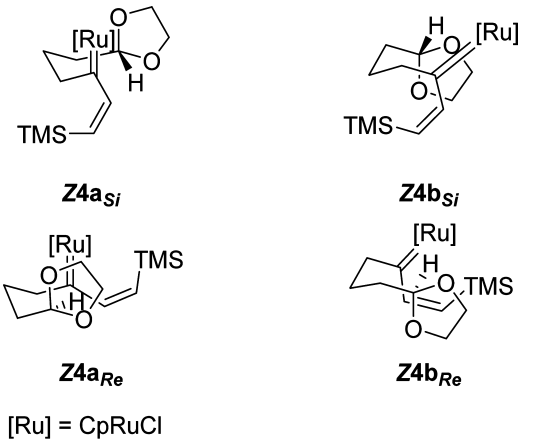

Figure 4. Suitable conformations for the hydride transfer to the ruthenium carbene in the case of isomer ***Z*4**.

We next tried to calculate the energy profiles for each of the 16 possible geometries found, but only 11 were connected with the final reaction products: ***Z*4a**$_{Si}$, ***Z*4b**$_{Re}$, ***E*4a**$_{Si}$, ***E*4b**$_{Si}$, ***E*4a**$_{Re}$, ***E*4b**$_{Re}$, ***E*5a**$_{Si}$, ***E*5b**$_{Si}$, ***E*5b**$_{Re}$, ***Z*5a**$_{Si}$,and ***Z*5b**$_{Si}$.[28]

The KMC study allowed us to determine the theoretical branching ratio of spiroacetals (***Z*3**/***E*3**) obtained as well as the preferred pathways. Considering that all molecules of the initially formed carbene species **2** are in the conformation represented by **2a**, the KMC simulations indicate that the system evolves almost exclusively to isomer ***E*3** (Figure 5).[29] Initially, the population of ruthenium carbene **2a** decreased to produce the η^3-vinyl carbene ***Z*4** and the most stable conformer **2c**, which quickly evolved to η^3-vinyl carbene ***E*5**. After 1.2×10^{-8} s all of the initial ruthenium carbene **2** was transformed into ***Z*4** and ***E*5** in a 7:93 ratio. After formation of ***E*5**, this intermediate started to evolve to the final product ***E*3**, which was produced in 93% yield through the paths involving intermediates ***E*5b**$_{Si}$ and ***E*5a**$_{Si}$ in a 83:10 ratio (Figure 5). Intermediate ***Z*4** had a longer lifetime, evolving after 2×10^{-3} s to the final product ***Z*3** in 7% yield through intermediates ***Z*4b**$_{Re}$ and ***Z*4a**$_{Si}$ in a 6:1 ratio.

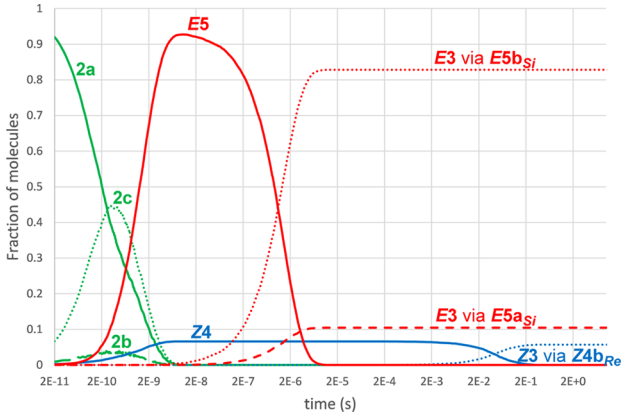

Figure 5. Fraction of molecules as a function of time obtained in the KMC simulations.

Thus, the main pathway to obtain ***E*3** involves the isomer ***E*5** and it goes through conformer ***E*5b**$_{Si}$ (Figure 6). The initial step

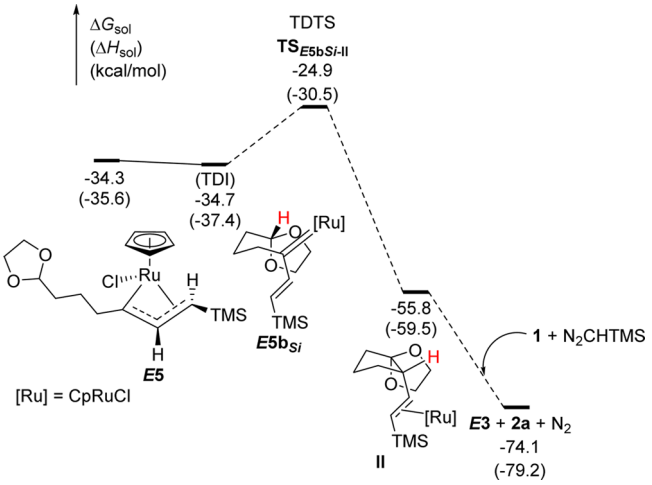

Figure 6. Free energy profile for the formation of ***E*3** from ***E*5** through conformer ***E*5b**$_{Si}$. Energies are relative to **2a** and are mass balanced.

is the conformational change of ***E*5** to the chairlike conformer ***E*5b**$_{Si}$, which is 0.4 kcal mol^{-1} more stable and more suitable for the hydride transfer.[30] Hydride migration to the *Si* face of the η^3-vinyl carbene ***E*5b**$_{Si}$ afforded species **II**, in which the ruthenium is η^2 coordinated to the alkene of the final product ***E*3** (ΔG° = −21.1 kcal mol^{-1}, $\Delta G^\ddagger$ = 9.8 kcal mol^{-1}). Decoordination of the ruthenium will afford free ***E*3**, while reaction of the metal species with **1** and (trimethylsilyl)-diazomethane regenerates catalytic species **2** with the evolution of N_2. The total ΔG° value for the formation of ***E*3** from **1** + N_2CHTMS is −74.1 kcal mol^{-1}.

The energetic span model of Kozuch and Shaik was also employed to calculate the energetic span (δE), the TOF-determining transition state (TDTS), the TOF-determining intermediate (TDI), and the TOF value for each of the calculated mechanistic pathways.[31] In this case, the energetic span for this pathway was 9.8 kcal mol^{-1} (where the TDI is ***E*5b**$_{Si}$ and the TDTS is the transition state for the hydride migration from ***E*5b**$_{Si}$ to **II**) and the calculated TOF was 2.8×10^5 s^{-1}. The other 10 possible pathways have both higher energetic span, δE, and smaller TOF,[32] which is in good agreement with the results of the KMC simulation and indicates that the path involving intermediate ***E*5b**$_{Si}$ is the most active for the studied transformation.

To support the reliability of the energy profiles calculated, further geometry optimizations and single-point energy calculations have been carried out using the ωB97XD functional[33] (which includes a version of Grimme's D2 dispersion corrections),[34] using the same basis sets and implicit solvent model as in the previous B3LYP-D3 study for (i) conformational analysis of ruthenium carbene **2**, (ii) formation of ***Z*4** and ***E*5** from **2a**,**c**, respectively, (iii) isomerization of ***Z*4**

DOI: 10.1021/acscatal.5b01333
ACS Catal. 2015, 5, 6255−6262

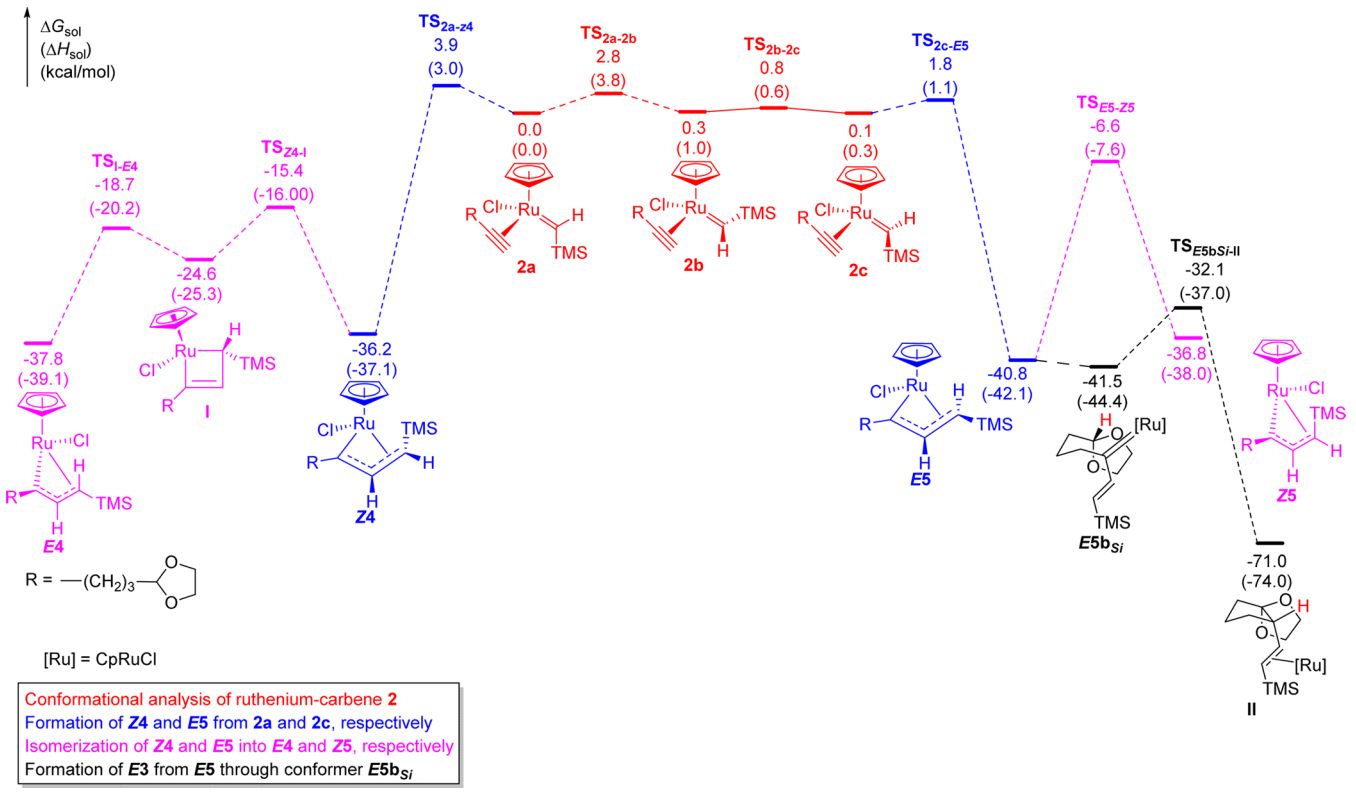

Figure 7. Free energy profile for the conformational analysis of **2**, formation of ***Z*4** and ***E*5** and their isomerization to ***E*4** and ***Z*5**, and the formation of ***E*3** from ***E*5** using the ωB97XD functional. Energies are relative to **2a** and are mass balanced.

and ***E*5** into ***E*4** and ***Z*5**, respectively, and (iv) formation of ***E*3** from ***E*5** through conformer $E5b_{Si}$ (Figure 7). Importantly, the results obtained using ωB97XD and B3LYP-D3 functionals show a very good agreement, reinforcing the confidence in the present computational study.

The KMC study for the profile calculated using the ωB97XD functional, showed in Figure 7, with all the initial molecules in conformation **2a** is displayed in Figure 8.[35] After 2×10^{-10} s **2a**

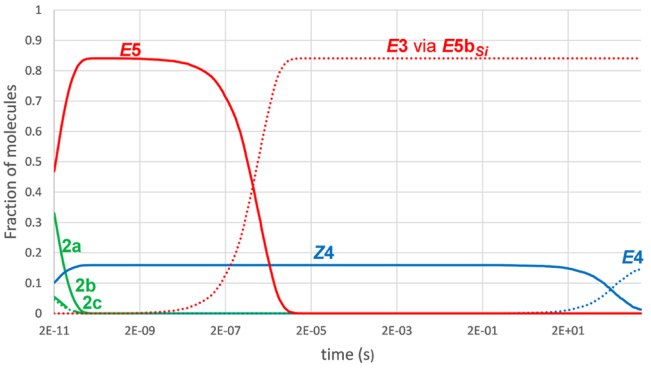

Figure 8. Fraction of molecules as a function of time obtained in the KMC simulations using the ωB97XD profile.

was completely transformed into ***Z*4** and ***E*5** in a 16:84 ratio. After formation of ***E*5**, this intermediate evolved to the final product ***E*3** in 84% yield through the intermediate $E5b_{Si}$ without any isomerization to ***Z*5**. Intermediate ***Z*4** evolved slowly to the more stable intermediate ***E*4** after 20 s.

Again, the kinetic results obtained from the ωB97XD and the B3LYP-D3 profiles agree very well, pointing out the robustness of the computational methodologies employed in the present study.

We subsequently turned our attention to the same reaction but using Cp*RuCl(cod) as catalyst, which showed the same stereoselectivity but gave better chemical yields.[10] As in the previous example, the conformational equilibrium of the initially formed ruthenium carbene species **2*** (Cp* instead of Cp) was analyzed (Figure 9). In this case, three conformational minima were also obtained but with a energy profile different from that when CpRuCl(cod) was used (Figure 1): the most stable conformer was complex **2a***, which has the bulky TMS group opposite to the Cp* ring, complex **2b***, which has the TMS group away from the

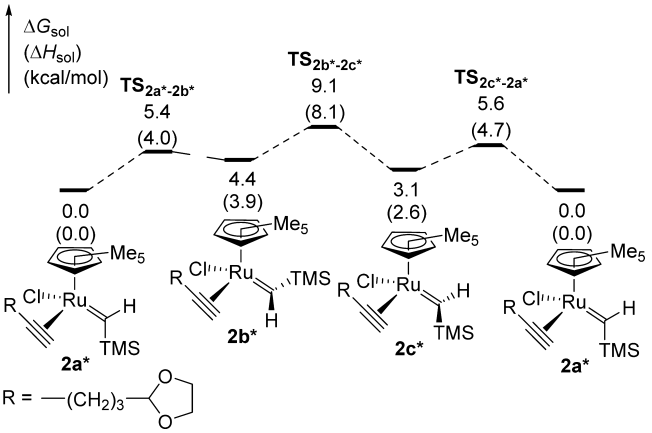

Figure 9. Free energy profile for conformational analysis of ruthenium carbene **2***. Energies are relative to **2a*** and are mass balanced.

DOI: 10.1021/acscatal.5b01333
ACS Catal. 2015, 5, 6255−6262

ruthenium alkyne ligand, was 4.4 kcal mol^{-1} less stable than **2a***, and complex **2c***, in which the TMS group is close to the ruthenium alkyne ligand, was 3.1 kcal mol^{-1} less stable than **2a***. The most unfavorable rotational isomerization, with $G^{\ddagger}$ = 9.1 kcal mol^{-1}, was obtained for the system in which the TMS group was located just beneath the Cp* ring (**2b*** → **2c***). The other two rotational isomerizations present lower energy barriers, with values for the Gibbs free energy of activation of 5.4 and 5.6 kcal mol^{-1} for **2a*** → **2b*** and **2c*** → **2a***, respectively (Figure 9).

We proceeded to evaluate the formation of the two η^3-vinyl carbene complexes ***Z4**** and ***E5**** from **2a*,c***, with ΔG° = −28.1 and −36.3 kcal mol^{-1} and $\Delta G^{\ddagger}$ = 8.0 and 7.7 kcal mol^{-1}, respectively (Figure 10).

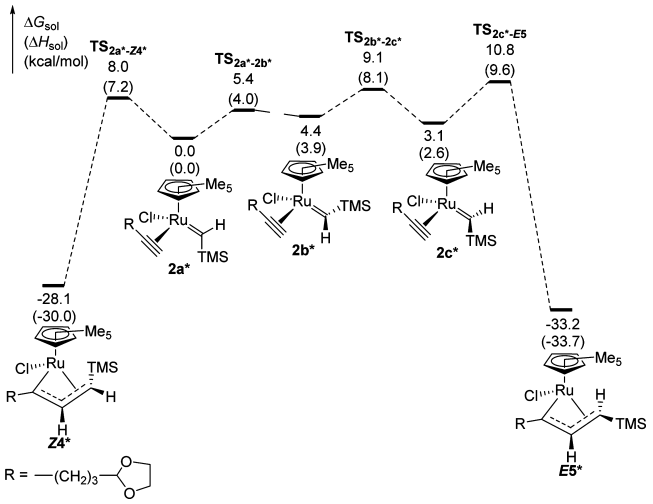

Figure 10. Free energy profile for the formation of ***Z4**** and ***E5**** from **2a*,c***, respectively. Energies are relative to **2a*** and are mass balanced.

Given the $\Delta G^{\ddagger}$ values shown in the energy profile for the formation of ***Z4**** and ***E5**** (Figure 10), it is reasonable to consider that most of the ruthenium carbene species **2*** will evolve through pathways involving intermediate ***Z4****. Thus, we first calculated the isomerization of ***Z4**** to ***E4**** via intermediate **I*** (Figure 11) and, as before, the pathways leading to ***Z3*** (through the conformers ***Z4a$_{Si}$**** and ***Z4b$_{Re}$****) and ***E3*** (through conformers ***E4a$_{Si}$****, ***E4b$_{Si}$****, ***E4a$_{Re}$**** and ***E4b$_{Re}$****) were evaluated.

KMC simulations including the six feasible pathways, bearing in mind once again that all molecules of the initially formed carbene species **2*** are in the conformation represented by **2a***,[36] show that ***E3*** is obtained exclusively (Figure 12). After approximately 1.5 × 10^{-6} s, all of the conformers of carbene **2*** had been transformed into ***Z4**** (99%) and ***E5**** (1%), thus showing that pathways involving intermediate ***E5**** can be ruled out. After 2 × 10^{-3} s, ***Z4**** started to isomerize to ***E4**** through intermediate **I***. Finally, ***E3*** was obtained in 94% yield via a pathway involving η^3-vinyl carbene ***E4b$_{Si}$**** (Figure 10). The other minor active pathways leading to **E3** involve the intermediate species ***E4a$_{Si}$**** and ***E4b$_{Re}$**** to give 3% and 1% yields, respectively. A minor amount of isomer ***Z3*** was also obtained through the pathway involving ***Z4a$_{Si}$*** (1% yield). In comparison to the mechanistic study with CpRuCl(cod), pathways leading to ***Z3*** were not active at all and there was almost a unique pathway to the final product ***E3***, which could

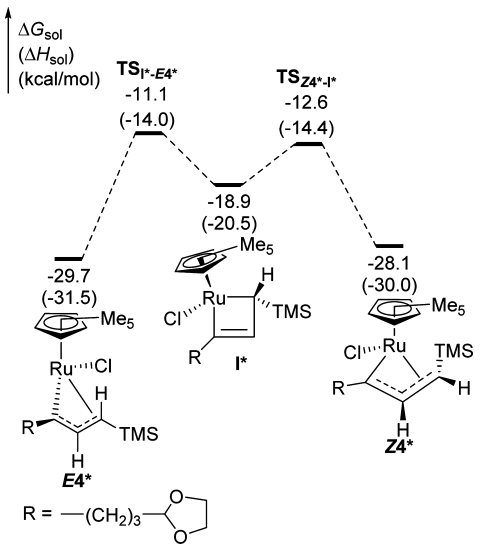

Figure 11. Free energy profiles for the isomerization of ***Z4**** to ***E4**** through Cp* ruthenacyclobutenes **I***. Energies are relative to **2a*** and are mass balanced.

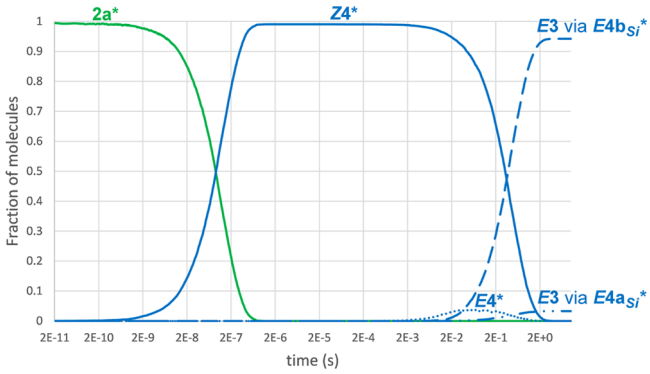

Figure 12. Fraction of molecules as a function of time obtained in the KMC simulations.

explain the better yields observed experimentally when Cp*RuCl(cod) is used.

The main pathway responsible for the major formation of ***E3*** involves the initial isomerization of η^3-vinyl carbene ***E4**** to its chairlike conformation ***E4b$_{Si}$****, which is 0.5 kcal mol^{-1} more stable,[37] followed by hydride migration over the *Si* face to give species **III** with ΔG° = −23.8 kcal mol^{-1} and $\Delta G^{\ddagger}$ = 15.3 kcal mol^{-1}. Finally, as in the case of the CpRuCl(cod), decoordination of the ruthenium will afford free ***E3*** (Figure 13).

The calculated energetic span, δE, for this pathway was 17.0 kcal mol^{-1}, where the TDI is ***Z4**** and the TDTS is the transition state for the isomerization step **I*** to ***E4****, showing that the rate-determining step in this case is the *Z* to *E* isomerization, rather than the hydride migration, the calculated TOF being 1.9 s^{-1}. The other six calculated pathways both have a higher energetic span, δE, and smaller TOF,[30] thus showing that the path involving the intermediate ***E4b$_{Si}$**** is the most active in the case where Cp*Ru(cod)Cl is used as catalyst.

In summary, we have calculated all pathways for the reaction of alkynyl acetal **1** with the ruthenium carbenes **2** and **2*** to give the spiroacetals ***Z3*** and ***E3*** (Scheme 4). Although both theoretical and experimental results show the exclusive formation of spiroacetal ***E3***, there are significant peculiarities

DOI: 10.1021/acscatal.5b01333
ACS Catal. 2015, 5, 6255−6262

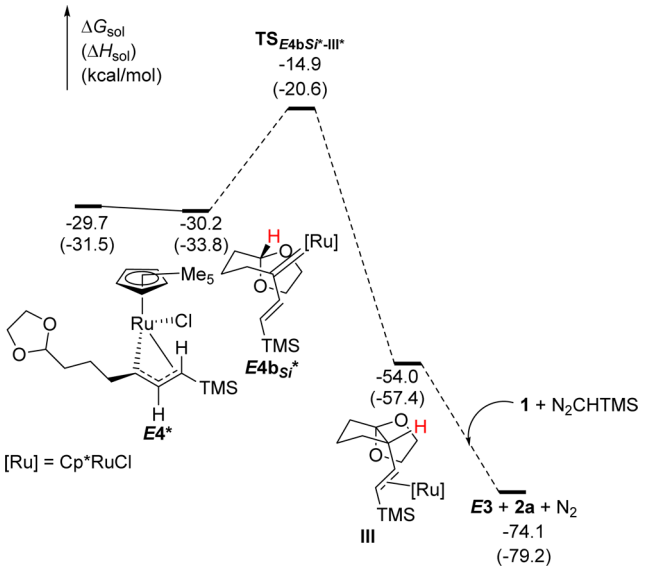

Figure 13. Free energy profile for the formation of ***E*3** from ***E*4*** through conformer ***E*4b$_{Si}$***. Energies are relative to **2a*** and are mass balanced.

in the mechanistic pathways depending on the catalyst used: (i) the conformational free energy profile for the two ruthenium carbene species **2** and **2*** is different in terms of both ΔG° and $\Delta G^{\ddagger}$ (Figure 1 vs Figure 9), and (ii) their transformations to either (*Z*)- or (*E*)-vinyl carbenes have different $\Delta G^{\ddagger}$ values (Figure 2 vs Figure 10). Therefore, with CpRu as catalyst, the main pathways go through the most favorable formation of intermediate ***E*5** and conformer ***E*5b$_{Si}$** (Figure 6). On the other hand, with Cp*Ru as catalyst, the initial formation of intermediate ***Z*4*** is favored (Figure 10) and its isomerization to ***E*4*** is faster than its transformation to the product ***Z*3** to finally afford ***E*3** through conformer ***E*4b$_{Si}$*** (Figure 13). KMC simulations and the energetic span model, δE, confirm these results. In conclusion, for a reaction that proceeds through a TMS-substituted ruthenium vinyl carbene as intermediate, the use of CpRu as catalyst should afford (*E*)-vinyl silanes as the major isomers, while the use of Cp*Ru should give rise to an *E*,*Z* configuration or a mixture depending on the evolution ($\Delta G^{\ddagger}$) of the initial (*Z*)-vinyl silane formed.[38]

■ ASSOCIATED CONTENT

Supporting Information

The Supporting Information is available free of charge on the ACS Publications website at DOI: 10.1021/acscatal.5b01333.

Optimized geometric parameters for all the calculated structures, nonactive pathways, and TOF calculations (PDF)

■ AUTHOR INFORMATION

Corresponding Authors

*E-mail for J.A.V.: jesus.varela@usc.es.
*E-mail for C.S.: carlos.saa@usc.es.

Notes

The authors declare no competing financial interest.

■ ACKNOWLEDGMENTS

The authors dedicate this article to Professor Agustí Lledós (Univ. Autònoma de Barcelona, Spain) on the occasion of his 60th birthday. This work was supported by MICINN (Spain) (projects CTQ2011-28258 and CTQ2014-51912REDC), Xunta de Galicia, and the European Regional Development Fund (projects GRC2014/032 and EM 2012/051). F.C. thanks XUGA for a predoctoral contract. We are also grateful to the CESGA (Xunta de Galicia) for computational time.

■ REFERENCES

(1) (a) Fürstner, A. *Science* **2013**, *341*, 1357. (b) Kress, S.; Blechert, S. *Chem. Soc. Rev.* **2012**, *41*, 4389−4408. (c) Kotha, S.; Dipak, M. K. *Tetrahedron* **2012**, *68*, 397−421. (d) Nolan, S. P.; Clavier, H. *Chem. Soc. Rev.* **2010**, *39*, 3305−3316. (e) Vougioukalakis, G. C.; Grubbs, R. H. *Chem. Rev.* **2010**, *110*, 1746−1787. (f) Hoveyda, A. H.; Malcolmson, S. J.; Meek, S. J.; Zhugralin, A. R. *Angew. Chem., Int. Ed.* **2010**, *49*, 34−44. (g) Grubbs, R. H. *Tetrahedron* **2004**, *60*, 7117−7140. (h) Connon, S. J.; Blechert, S. *Angew. Chem., Int. Ed.* **2003**, *42*, 1900−1923.

(2) (a) Fox, H. H.; Wolf, M. O.; O'Dell, R.; Lin, B. L.; Schrock, R. R.; Wrighton, M. S. *J. Am. Chem. Soc.* **1994**, *116*, 2827−2843. (b) Katz, T. J.; Sivavec, T. M. *J. Am. Chem. Soc.* **1985**, *107*, 737−738. (c) Masuda, T.; Higashimura, T. *Acc. Chem. Res.* **1984**, *17*, 51−56.

(3) (a) Li, J.; Lee, D. *Eur. J. Org. Chem.* **2011**, *2011*, 4269−4287. (b) Katz, T. J. *Angew. Chem., Int. Ed.* **2005**, *44*, 3010−3019. (c) Diver, S. T.; Giessert, A. J. *Chem. Rev.* **2004**, *104*, 1317−1382.

(4) Rubin, M.; Rubina, M.; Gevorgyan, V. *Chem. Rev.* **2007**, *107*, 3117−3179.

(5) Vovard-Le Bray, C.; Dérien, S.; Dixneuf, P. H. *C. R. Chim.* **2010**, *13*, 292−303.

(6) Paih, J. L.; Bray, C. V.-L.; Dérien, S.; Dixneuf, P. H. *J. Am. Chem. Soc.* **2010**, *132*, 7391−7397.

(7) Vovard-Le Bray, C.; Dérien, S.; Dixneuf, P. H. *Angew. Chem., Int. Ed.* **2009**, *48*, 1439−1442.

(8) Monnier, F.; Vovard-Le Bray, C.; Castillo, D.; Aubert, V.; Dérien, S.; Dixneuf, P. H.; Toupet, L.; Ienco, A.; Mealli, C. *J. Am. Chem. Soc.* **2007**, *129*, 6037−6049.

(9) Vovard-Le Bray, C.; Dérien, S.; Dixneuf, P. H.; Murakami, M. *Synlett* **2008**, *2008*, 193−196.

(10) Cambeiro, F.; López, S.; Varela, J. A.; Saá, C. *Angew. Chem., Int. Ed.* **2012**, *51*, 723−727.

(11) Cambeiro, F.; López, S.; Varela, J. A.; Saá, C. *Angew. Chem., Int. Ed.* **2014**, *53*, 5959−5963.

(12) Frisch, M. J.; Trucks, G. W.; Schlegel, H. B.; Scuseria, G. E.; Robb, M. A.; Cheeseman, J. R.; Scalmani, G.; Barone, V.; Mennucci, B.; Petersson, G. A.; Nakatsuji, H.; Caricato, M.; Li, X.; Hratchian, H. P.; Izmaylov, A. F.; Bloino, J.; Zheng, G.; Sonnenberg, J. L.; Hada, M.; Ehara, M.; Toyota, K.; Fukuda, R.; Hasegawa, J.; Ishida, M.; Nakajima, T.; Honda, Y.; Kitao, O.; Nakai, H.; Vreven, T.; Montgomery, J. A., Jr.; Peralta, J. E.; Ogliaro, F.; Bearpark, M.; Heyd, J. J.; Brothers, E.; Kudin, K. N.; Staroverov, V. N.; Kobayashi, R.; Normand, J.; Raghavachari, K.; Rendell, A.; Burant, J. C.; Iyengar, S. S.; Tomasi, J.; Cossi, M.; Rega, N.; Millam, N. J.; Klene, M.; Knox, J. E.; Cross, J. B.; Bakken, V.; Adamo, C.; Jaramillo, J.; Gomperts, R.; Stratmann, R. E.; Yazyev, O.; Austin, A. J.; Cammi, R.; Pomelli, C.; Ochterski, J. W.; Martin, R. L.; Morokuma, K.; Zakrzewski, V. G.; Voth, G. A.; Salvador, P.; Dannenberg, J. J.; Dapprich, S.; Daniels, A. D.; Farkas, Ö.; Foresman, J. B.; Ortiz, J. V.; Cioslowski, J.; Fox, D. J. *Gaussian 09, Revision D.01*; Gaussian, Inc., Wallingford, CT, 2013.

(13) (a) Parr, R. G.; Wang, Y. *Density Functional Theory of Atoms and Molecules*; Oxford University Press: New York, 1989. (b) Becke, A. D. *J. Chem. Phys.* **1993**, *98*, 5648−5652. (c) Miehlich, B.; Savin, A.; Stoll, H.; Preuss, H. *Chem. Phys. Lett.* **1989**, *157*, 200−206. (d) Lee, C.; Yang, W.; Parr, R. G. *Phys. Rev. B: Condens. Matter Mater. Phys.* **1988**, *37*, 785−789.

(14) Hay, P. J.; Wadt, W. R. *J. Chem. Phys.* **1985**, *82*, 299−310.

(15) Hay, P. J.; Wadt, W. R. *J. Chem. Phys.* **1985**, *82*, 270−283.

(16) (a) Gordon, M. S. *Chem. Phys. Lett.* **1980**, *76*, 163−168. (b) Hariharan, P. C.; Pople, J. A. *Mol. Phys.* **1974**, *27*, 209−214. (c) Hariharan, P. C.; Pople, J. A. *Theor. Chim. Acta* **1973**, *28*, 213−222.

DOI: 10.1021/acscatal.5b01333
ACS Catal. 2015, 5, 6255−6262

(d) Hehre, W. J.; Ditchfield, R.; Pople, J. A. *J. Chem. Phys.* **1972**, *56*, 2257−2261. (e) Ditchfield, R.; Hehre, W. J.; Pople, J. A. *J. Chem. Phys.* **1971**, *54*, 724−728.
(17) Grimme, S.; Antony, J.; Ehrlich, S.; Krieg, H. *J. Chem. Phys.* **2010**, *132*, 154104.
(18) Marenich, A. V.; Cramer, C. J.; Truhlar, D. G. *J. Phys. Chem. B* **2009**, *113*, 6378−6396.
(19) (a) McLean, A. D.; Chandler, G. S. *J. Chem. Phys.* **1980**, *72*, 5639−5648. (b) Krishnan, R.; Binkley, J. S.; Seeger, R.; Pople, J. A. *J. Chem. Phys.* **1980**, *72*, 650−654.
(20) (a) Bortz, A. B.; Kalos, M. H.; Lebowitz, J. L. *J. Comput. Phys.* **1975**, *17*, 10−18. (b) Gillespie, D. T. *J. Comput. Phys.* **1976**, *22*, 403−434. The Fortran90 code used for the KMC simulations is included in the Supporting Information.
(21) Eyring, H. *J. Chem. Phys.* **1935**, *3*, 107−115.
(22) Eckart, C. *Phys. Rev.* **1930**, *35*, 1303−1309.
(23) Malick, D. K.; Petersson, G. A.; Montgomery, J. A., Jr. *J. Chem. Phys.* **1998**, *108*, 5704−5713.
(24) The conformation of the carbene ligand−ruthenium bond has been found to be important for the metathesis activity of ruthenium carbene catalysts: (a) Straub, B. F. *Angew. Chem., Int. Ed.* **2005**, *44*, 5974−5978. (b) Straub, B. F. *Adv. Synth. Catal.* **2007**, *349*, 204−214.
(25) From **2b** no transition state to η^3-vinylcarbene complex was found.
(26) Ruthenacyclobutenes have been discarded as intermediates in the enyne metathesis reaction; see: (a) Lippstreu, J. J.; Straub, B. F. *J. Am. Chem. Soc.* **2005**, *127*, 7444−7457. For an experimental observation of a cobaltacyclobutene−η^3-vinylcarbene equilibration, see: (b) O'Connor, J. M.; Baldridge, K. K.; Vélez, C. L.; Rheingold, A. L.; Moore, C. E. *J. Am. Chem. Soc.* **2013**, *135*, 8826−8829.
(27) (a) Seeman, J. I. *Chem. Rev.* **1983**, *83*, 83−134. (b) Seeman, J. I. *J. Chem. Educ.* **1986**, *63*, 42.
(28) For the 11 calculated reaction profiles, see the Supporting Information.
(29) KMC simulations considering all the initial molecules in conformations **2b**,**c** and using calculated values of *G* with one or no decimal gave essentially the same results; see the Supporting Information for details.
(30) The missing transition states between the intermediate ***E*5** and its conformer ***E*5b**$_{Si}$ were not determined, as they correspond to low energy barriers and their influence is negligible in the total energy profile: Uhe, A.; Kozuch, S.; Shaik, S. *J. Comput. Chem.* **2011**, *32*, 978−985.
(31) Kozuch, S.; Shaik, S. *Acc. Chem. Res.* **2011**, *44*, 101−110.
(32) For calculated energetic spans (δE) and TOF values of all the pathways, see the Supporting Information.
(33) Chai, J.-D.; Head-Gordon, M. *Phys. Chem. Chem. Phys.* **2008**, *10*, 6615−6620.
(34) Grimme, S. *J. Comput. Chem.* **2006**, *27*, 1787−1799.
(35) KMC simulations considering all the initial molecules in conformations **2b**,**c** gave slightly different results due to the small $\Delta\Delta G^{\ddagger}$ value between $\mathbf{TS}_{\mathbf{2a\text{-}Z4}}$ and $\mathbf{TS}_{\mathbf{2a\text{-}2b}}$ using the ωB97DX rather than the B3LYP-D3 functional. The use of calculated values of *G* with only one or no decimal gave essentially the same results; see the Supporting Information for details.
(36) KMC simulations considering all the initial molecules in conformations **2b*** or **2c*** and using calculated values of *G* with one or no decimal gave essentially the same results; see Supporting Information for details.
(37) The missing transition states between the intermediate ***E*4*** and its conformer ***E*4b**$_{Si}$* were not determined; see ref 30.
(38) The changes observed might be attributed to the distinct steric effects of Cp and Cp*. For a related example of these drastic steric effects, see: Oakdale, J. S.; Sit, R. K.; Fokin, V. V. *Chem. - Eur. J.* **2014**, *20*, 11101−11110.

DOI: 10.1021/acscatal.5b01333
ACS Catal. 2015, 5, 6255−6262